

Communication

Processing-Speed Enhancement in a Delay-Laser-Based Reservoir Computer by Optical Injection

Ziyue Li, Song-Sui Li ^{*}, Xihua Zou, Wei Pan and Lianshan Yan

School of Information Science and Technology, Southwest Jiaotong University, Chengdu 610031, China; zyli@my.swjtu.edu.cn (Z.L.); zouxihua@swjtu.edu.cn (X.Z.); wpan@swjtu.edu.cn (W.P.); lsyan@swjtu.edu.cn (L.Y.)
^{*} Correspondence: ssl@swjtu.edu.cn

Abstract: A delay-laser-based reservoir computer (RC) usually has its processing speed limited by the transient response of laser dynamics. Here, we study a simple all-optical approach to enhancing the processing speed by introducing optical injection to the reservoir layer of conventional RC that consists of a semiconductor laser with a delay loop. Using optical injection, the laser's transient response effectively accelerates due to the speeded carrier-photon resonance. In the chaotic time-series prediction task, the proposed RC achieves good performance in a flexible range of injection detuning frequency under sufficient injection rate. Using proper injection parameters, the prediction error is significantly reduced and stabilized when using high processing speed. For achieving a prediction error below 0.006, the optical injection enhances the processing speed by an order of magnitude of about 5 GSample/s. Moreover, the proposed RC extends the advantage to the handwritten digit recognition task by achieving better word error rate.

Keywords: reservoir computer (RC); semiconductor laser; optical injection; chaotic time-series prediction; handwritten digit recognition; processing speed



Citation: Li, Z.; Li, S.-S.; Zou, X.; Pan, W.; Yan, L. Processing-Speed Enhancement in a Delay-Laser-Based Reservoir Computer by Optical Injection. *Photonics* **2022**, *9*, 240. <https://doi.org/10.3390/photonics9040240>

Received: 1 March 2022

Accepted: 1 April 2022

Published: 4 April 2022

Publisher's Note: MDPI stays neutral with regard to jurisdictional claims in published maps and institutional affiliations.



Copyright: © 2022 by the authors. Licensee MDPI, Basel, Switzerland. This article is an open access article distributed under the terms and conditions of the Creative Commons Attribution (CC BY) license (<https://creativecommons.org/licenses/by/4.0/>).

1. Introduction

Conventional computers or Turing approaches are inefficient to solve complex and abstract problems such as pattern recognition or time series prediction [1–4]. Solving abstract tasks are often achieved using algorithms related to artificial intelligence where learning-based computation schemes are adopted. Nonetheless, the computing efficiency and processing speed are difficult to be further improved by only optimizing algorithms or electronic circuits [5]. Photonic devices are usually fast and power efficient. Recently, utilizing transient response of nonlinear photonic device attracted considerable attentions for achieving learning-based fast computing with high efficiency [6–25]. As one of the most popular photonic implementations of learning-based computation, a delay-laser-based reservoir computer (RC) utilizes nonlinear transient of a semiconductor laser under delayed feedback [7]. Similar to the famously demonstrated echo state network in [8], a delay-laser-based RC retains the advantage that only the connections from reservoir to output layer are required to be trained [9–18]. Moreover, better than the echo state network where real nodes are required, a delay-laser-based RC has virtual nodes along the delay loop which obviously simplifies the configuration and reduces the cost [7].

In the last decade, Brunner et al. pioneered a delay-laser-based RC architecture where the input signal multiplied with a temporal mask was added to the delayed feedback laser on either bias current or optical intensity [7]. Here, the input signal is a series of discrete data with a holding time of T . The temporal mask has a period equaling to $T = N\theta$ where N and θ , respectively, correspond to the number and interval of virtual nodes within the delay loop. The number of nodes N ranging from tens to hundreds is typically sufficient for the tasks such as pattern recognition or time series prediction [17]. Meanwhile, the interval time θ should be limited within a range related to the characteristic transient response time

τ_{tr} to enable nonlinear connections between neighboring virtual nodes [19–21]. In order to enhance the processing speed, the conventional approach is using parallel processing method where multiple coupled or uncoupled delay-laser-based RCs were integrated [17]. Compatible with the parallel processing method, improving single RC processing speed using phase-to-intensity coupling response was also demonstrated [19]. Besides single-mode dynamics, dual-mode dynamics such as polarization dynamics from a VCSEL using polarization-controlled optical feedback is investigated as well [25]. Fundamentally, the delay-laser-based RC architecture has a processing speed which is inversely proportional to the interval θ for a given N . As θ has a lower limit related to τ_{tr} , reducing τ_{tr} should be a promising solution towards processing-speed enhancement.

In this work, we propose and numerically demonstrated a simple all-optical approach for enhancing processing speed of a delay-laser-based RC by optical injection. In the reservoir layer, a response laser under delayed optical feedback is optically injected by a master laser. Due to proper optical injection, the carrier-photon resonance can be sped up to accelerate the transient response, hence enhancing the processing speed in chaotic time-series prediction and handwritten digit recognition tasks.

2. Methods

Figure 1 shows a schematic of the proposed system. The input and output layers have similar configurations to the conventional RC, whereas the reservoir layer is modified by introducing optical injection from a master laser to the delayed feedback response laser. The response laser in Figure 1b is described by the slowly varying complex electric field amplitude $E(t)$ and the carrier density $N(t)$. The rate equations that govern the laser dynamics are based on the modified Lang-Kobayashi equations [26]:

$$\frac{dE(t)}{dt} = \frac{1}{2}(1 + i\alpha) \left\{ \frac{G_N(N(t) - N_0)}{1 + \varepsilon|E(t)|^2} - \frac{1}{\tau_p} \right\} E(t) + k_s \sqrt{I_s} \exp\{i\pi S(t)\} \exp(2\pi i \times \Delta v_s t) + k_f E(t - \tau) \exp(-i2\pi\nu_0\tau) + k_i \sqrt{I_i} \exp(2\pi i \times \Delta v_i t), \tag{1}$$

$$\frac{dN(t)}{dt} = J - \frac{N(t)}{\tau_s} - \frac{G_N(N(t) - N_0)}{1 + \varepsilon|E(t)|^2} |E(t)|^2, \tag{2}$$

where the linewidth enhancement factor α , the gain coefficient G_N , the carrier density at transparency N_0 , the photon lifetime τ_p , the carrier lifetime τ_s , the gain saturation coefficient ε , and the bias current J are the parameters of the response laser and summarized in Table 1 [20]. At the right-hand side of Equation (1), the input layer, delayed optical feedback, and optical injection are, respectively, described by the second, third, and last terms. To focus on the dynamics, the effect of spontaneous emission noise is not taken into account in this work. Though the spontaneous emission noise of response laser may be detrimental to the RC performance, as it induces consistency problem if the response laser is in chaotic state. Nonetheless, as demonstrated by [20], a proper stable locking state by introducing optical injection to the delayed feedback response laser is helpful to minimize the effect from noise.

In Figure 1a, the input layer couples the masked signal $S(t)$ to the optical phase of response laser using a coherent light source with coupling strength k_s and coupling detuning frequency Δv_s . $S(t)$ is generated by multiplying the information $u(n)$ to a temporal mask $mask(t)$. γ is used for adjusting the standard deviation of the mask [20]. Hence, the masked signal can be described as $S(t) = \gamma \times mask(t) \times u(n)$. $\Delta v_s = -4.7$ GHz is adopted to prepare for a stable locking condition when $S(t)$ is turned off throughout the work [20,21].

In Figure 1b, to form a reservoir with virtual nodes, a delayed optical feedback loop with delay time τ is used to mimic N connected nodes. The feedback rate is set to $k_f = 9 \text{ ns}^{-1}$ to enable nonlinear connections between these virtual nodes throughout this work. To enhance the transient dynamics of response laser, an optical injection from a master laser is specified by the injection rate k_i and the injection detuning frequency

Δv_i . $\Delta v_i = v_i - v_0$, where $v_{i,0}$ represent the free-running optical frequency of the master and response lasers.

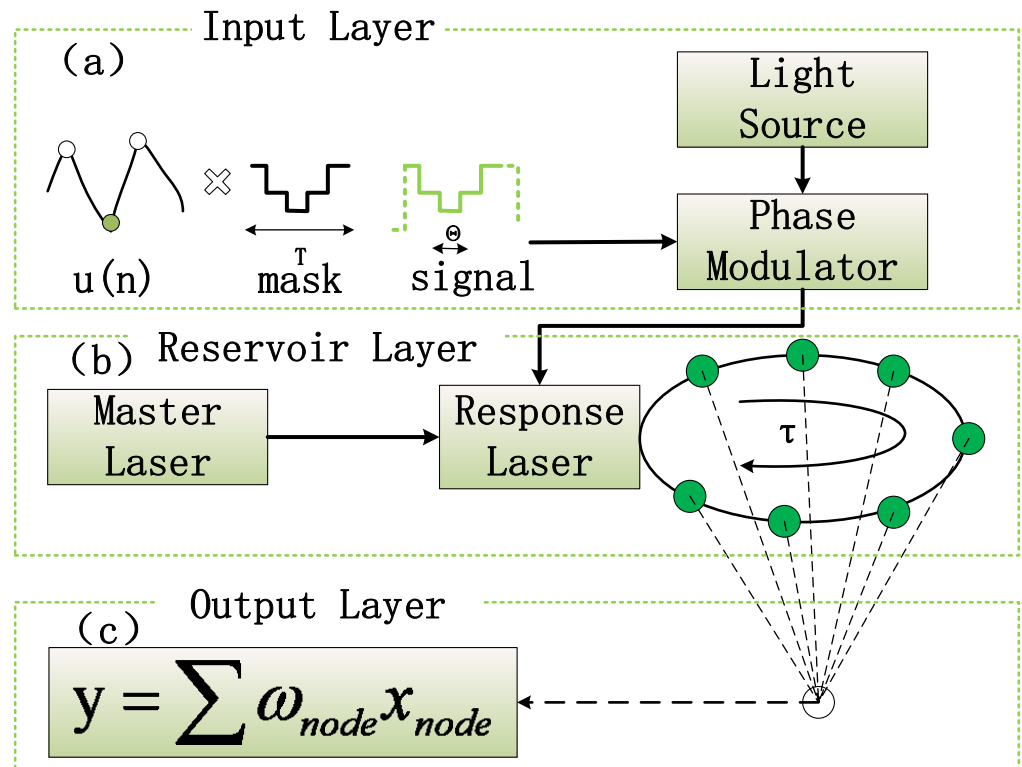


Figure 1. Schematic of the proposed system including (a) input layer, (b) reservoir layer, (c) output layer.

Table 1. Values of laser parameters.

Parameters	Designation	Value
Linewidth enhancement factor	α	3
Gain coefficient	G_N	$8.4 \times 10^{-13} \text{ m}^3 \text{ s}^{-1}$
Carrier density at transparency	N_0	$1.4 \times 10^{24} \text{ m}^{-3}$
Gain saturation	ϵ	2.0×10^{-23}
Injection current of the response laser	J	$1.05 \times 10^{33} \text{ m}^{-3} \text{ s}^{-1}$
Carrier lifetime	τ_s	2.04 ns
Photon lifetime	τ_p	1.927 ps
Intensity of light source/master laser	$I_{s,i}$	6.56×10^{20}
Coupling strength of light source	k_s	14 ns^{-1}
Coupling detuning frequency of light source	Δv_s	-4.7 GHz
Injection rate of master laser	k_i	Scanning over 0–14 ns ⁻¹
Detuning frequency of master laser	Δv_i	Scanning over -40–40 GHz
Node number of delay loop	N	100
Interval of node	θ	Scanning over 1–20 ps
Holding time in input layer	T	$T = N\theta$
Loop delay time	τ	$\tau = T + \theta$

In Figure 1c of the output layer, as for the training procedure, the states (values of intensity) of virtual nodes x_{node} in the reservoir layer are adopted to train and optimize the weights ω_{node} based on the commonly used ridge regression algorithm. As for the prediction procedure, the states x_{node} and the optimized ω_{node} are used to calculate the prediction $y = \sum \omega_{node} x_{node}$.

If the injection rate k_i is set to zero, the rate equations in Equations (1) and (2) are reduced to a conventional delay-laser-based RC. The numerical results are calculated using the fourth-order Runge–Kutta method with time step 0.1 ps.

3. Transient Dynamics of Response Laser

As mentioned in [20], the best performance on time-series prediction task prefers the delayed feedback response laser being injection locked to the coherent light source when the masked signal is turned off [$S(t) = 0$]. In this work, the transient response time τ_{tr} represents the characteristic time of the impulse response of such locked response laser. When $S(t) = 0$, for feedback parameters of $\tau = 0.303$ ns and $k_f = 9$ ns⁻¹, the response laser stays in stable locking state when using $k_s = 14$ ns⁻¹ for with ($k_i = 12$ ns⁻¹, $\Delta\nu_i = \Delta\nu_s$) and without ($k_i = 0$ ns⁻¹) master laser injection. Though the response laser outputs constant intensities for both cases [27,28], the autocorrelation of its impulse response in Figure 2a shows damped oscillations at different time scales. The transient response time τ_{tr} corresponds to the period of such oscillation, which is obviously sensitive to the injection from the master laser. It is worth mentioning that the impulse response partially repeats itself after every feedback delay time τ , which is generally observed in chaotic states as a time delay signature [29]. For delay-laser-based RC systems, using asynchronization between the holding time T and delay time τ is a popular approach which may also be helpful to reduce the potential threat of such time delay signature [9,20,21].

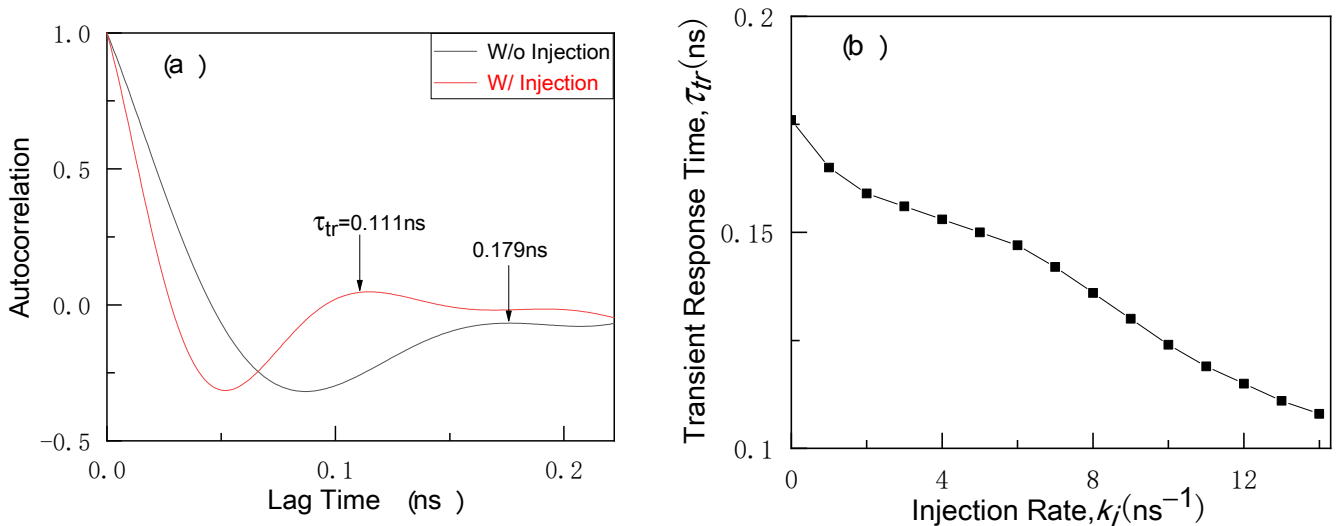


Figure 2. (a) Autocorrelation of the impulse response of response laser with ($k_i = 12$ ns⁻¹, $\Delta\nu_i = \Delta\nu_s$) and without ($k_i = 0$ ns⁻¹) master laser injection. (b) Transient response time τ_{tr} as a function of injection rate k_i .

Optical injection has been massively investigated for speeding up carrier-photon resonance and enhancing modulation bandwidth of semiconductor lasers, which should also be helpful to manipulate the transient response time τ_{tr} [30,31]. In Figure 2a, τ_{tr} reduces from 0.179 ns to 0.111 ns when the injection from master laser is introduced, which reveals an effectively accelerated transient response. Such acceleration is due to the speeded carrier-photon resonance by optical injection. To further confirm the result, the variation of τ_{tr} is showed in Figure 2b. As the injection rate k_i from the master laser increases, τ_{tr} is effectively reduced. However, if k_i is too large, exceeding 30 ns⁻¹, reduction in τ_{tr} is saturated, which is not plotted in Figure 2b. The reduction in τ_{tr} provides more room for reducing θ , hence resulting in a higher processing speed of RC.

4. Results

4.1. Chaotic Time-Series Prediction

Classical tasks for testing RC performance include digital or pattern recognition, nonlinear channel equalization, chaotic time-series prediction, etc.. Chaotic time-series prediction is one of the most popular tasks, as it examines both the memory capacity and nonlinearity [32]. In this work, chaotic time-series prediction is adopted to test RC

performance in terms of accuracy and processing speed. The Sante Fe data, corresponding to the intensity time-series of a chaotic far-infrared laser, are adopted as the information $u(n)$ to be processed in the task [33]. The discrete sequence has 4000 data points where the first 3000 are used for training and the rest are used for testing [34]. Each data point has a holding time of $T = N\theta$ and is masked by an N -points random mask with six discrete levels $(-1, -0.6, -0.2, 0.2, 0.6, 1)$ [14]. The mask is used to maintain the high dimensionality between the input layer and the reservoir layer. Then, the masked signal is phase-modulated to the coherent light source and coupled to the phase dynamics of response laser in the reservoir layer. The states of virtual nodes are collected by measuring the intensity dynamics at each virtual node. The task is a one-step ahead prediction in which a former data point is processing in RC to predict a latter one. Thus, the processing speed is evaluated as T^{-1} . The prediction performance is evaluated by the normalized mean square error (NMSE) defined as follows:

$$NMSE = \frac{1}{m} \frac{\sum_{j=1}^m [y(j) - \bar{y}(j)]^2}{\sigma(\bar{y})}, \quad (3)$$

where j is the index of the input data, and m is the total number of data. $y(j)$ is the output of the RC. $\bar{y}(j)$ is the original target value. Practically, the performance is considered to be good if the NMSE is below 0.1 [12,19]. For the virtual nodes within the delay loop, the number is set to $N = 100$, which is typically sufficient for tasks such as time-series prediction [16]. Asynchronization configuration of $\tau = T + \theta$ between the delay time τ and holding time T is adopted [9,20,21,32,35,36].

When using a small interval of $\theta = 3$ ps, the processing speed is $T^{-1} = 3.3$ GSample/s. Under $k_s = 14 \text{ ns}^{-1}$, Figure 3 compares the prediction performance between the conventional and proposed RCs corresponding to Figure 2. In Figure 3a, the conventional RC produces significant prediction errors between the theory and the prediction waveforms shown by the green curve, and the measured NMSE is relatively large, at about 0.0468. Such a poor performance is related to the reduced nonlinearity of connections between nodes when θ is too small. By contrast, the proposed optical injection effectively accelerates the transient response in Figure 2, which significantly reduces the prediction errors at high-speed processing, hence improving the NMSE performance by an order of magnitude of more than 0.0016 in Figure 3b.

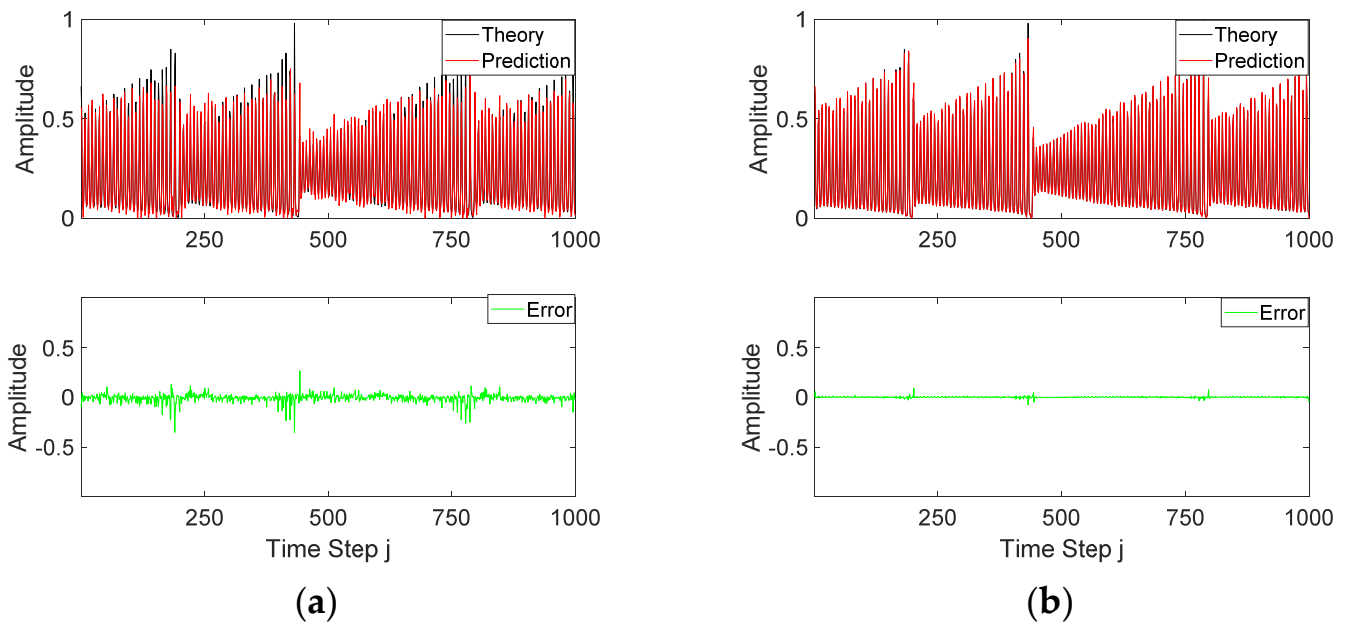


Figure 3. Temporal theory (black) and prediction (red) waveforms, and prediction error (green) from (a) conventional RC and (b) proposed RC. The interval of $\theta = 3$ ps corresponds to a processing speed of about $T^{-1} = 3.3$ GSample/s.

4.1.1. Dependencies on Injection Parameters

Figure 3 shows that the proposed RC has a better performance than conventional RC in high-speed processing. The dependencies of this improvement on injection parameters are further investigated by Figures 4 and 5. To eliminate the randomness of the mask, the plotted NMSE data are the mean values in 10 runs of different masks.

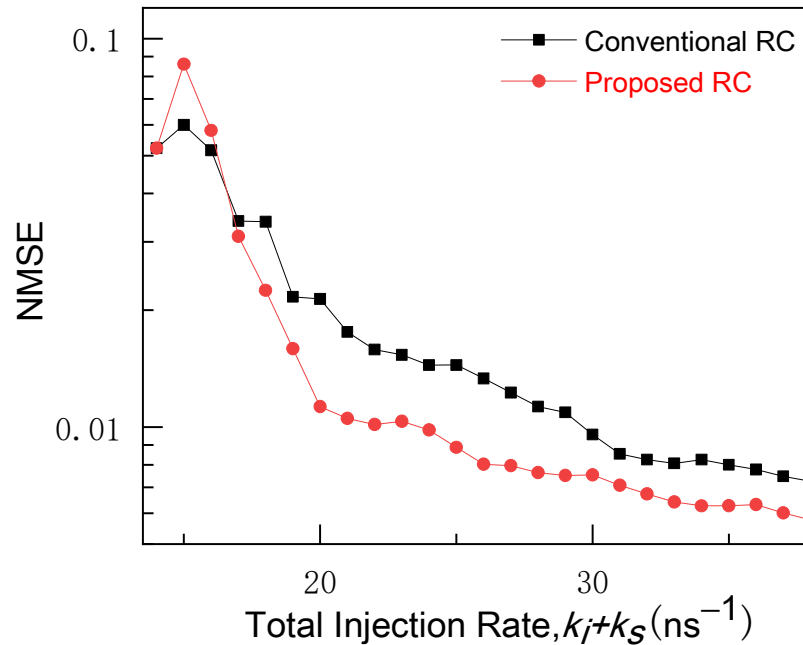


Figure 4. Measured NMSE as a function of total injection rate $k_i + k_s$ for conventional (black) and proposed (red) RCs. The data from conventional RC are obtained by setting $k_i = 0$. The data from proposed RC are obtained by setting $k_s = 14 \text{ ns}^{-1}$ and $\Delta\nu_i = \Delta\nu_s$.

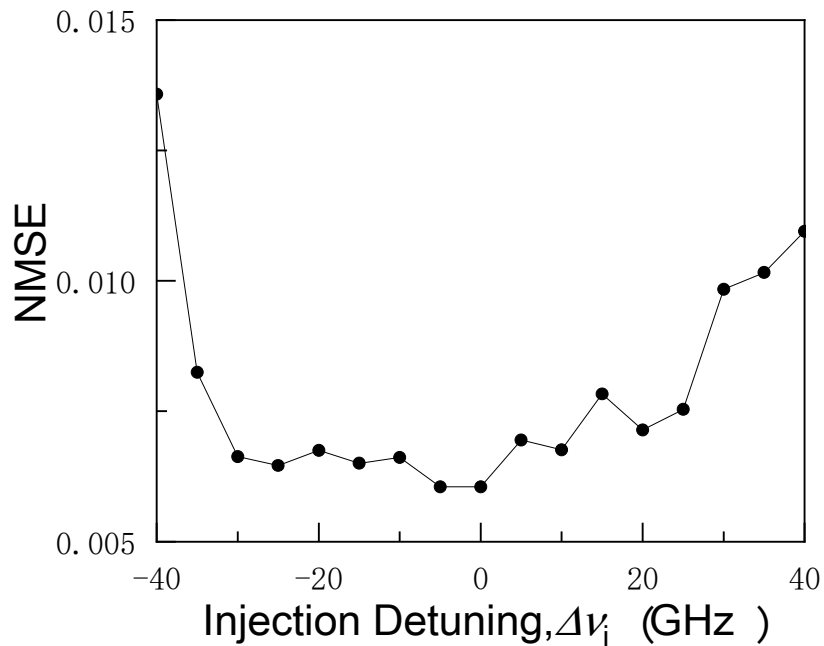


Figure 5. Measured NMSE as a function of $\Delta\nu_i$ when $k_i = 12 \text{ ns}^{-1}$ and $k_s = 14 \text{ ns}^{-1}$.

Figure 4 plots the NMSE as a function of the total injection rate $k_i + k_s$. The data shown in red are obtained from the proposed RC by varying k_i for $k_s = 14 \text{ ns}^{-1}$ and $\Delta\nu_i = \Delta\nu_s$, whereas those in black are obtained from the conventional RC by varying k_s for $k_i = 0$.

The interval of $\theta = 3$ ps corresponds to a processing speed of about $T^{-1} = 3.3$ GSample/s. Interestingly, comparing the red to black under same total injection rates, the proposed RC always achieves better NMSE performance when $k_i + k_s > 17$ ns⁻¹. As the injection from master laser has no phase modulation, it only contributes to the acceleration of transient speed without impairments on the phase dynamics. Figure 4 reveals that using injection from the master laser is better than just adjusting the coupling from the coherent light source.

To further examine the dependence on the injection detuning frequency $\Delta\nu_i$, Figure 5 plots the NMSE as a function of $\Delta\nu_i$ when $k_i = 12$ ns⁻¹ and $k_s = 14$ ns⁻¹. The interval time is $\theta = 10$ ps. Obviously, the NMSE is sensitive to $\Delta\nu_i$ as $\Delta\nu_i$ varies from -40 GHz to 40 GHz. Particularly, the NMSE performance prefers proper range of negative $\Delta\nu_i$. For instance, the NMSE is smaller at detuning frequencies within -30 GHz $< \Delta\nu_i < 0$ than that at detuning frequencies outside. This flexible range significantly improves the robustness of the RC performances as the detuning frequency often has fluctuations due to temperature instabilities in practice, which will be further verified experimentally in the future work.

4.1.2. Processing-Speed Enhancement

To investigate the enhancement on the processing speed, Figure 6 plots the NMSE as a function of processing speed T^{-1} . The processing speed T^{-1} is varied through adjusting the interval time θ . The data shown in black are measured from the conventional RC with $k_s = 14$ ns⁻¹, whereas that shown in red are measured from the proposed RC by further involving $k_i = 12$ ns⁻¹ and $\Delta\nu_i = \Delta\nu_s$. Fluctuations in NMSE are observed in the conventional RC, which are also reported by previous works [19,37]. Since the RC performance is strongly related to the dynamics of response laser, the fluctuation of NMSE may be related to the perturbation of dynamical states due to varying the feedback delay time. Comparing the red to black, the proposed RC shows comparable NMSE performance to that of the conventional RC for a relatively slow processing speed of $T^{-1} < 630$ MSample/s. Interestingly, for a relatively high processing speed of $T^{-1} > 630$ MSample/s, the proposed RC still retains good NMSE performance, whereas the conventional RC fails. For instance, to retain the NMSE of less than 0.006, the conventional RC has an upper limit of a processing speed of about $T^{-1} = 500$ MSample/s. By contrast, the proposed RC can increase the processing speed by about an order of magnitude to 5 GSample/s. The processing-speed enhancement is still valid even when the same total injection rate are adopted. In addition, the proposed RC significantly improves the stability of NMSE performance when tuning the processing speed.

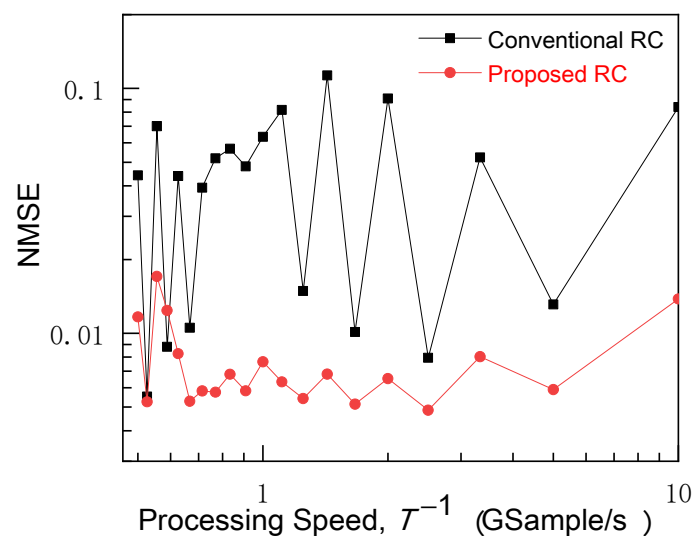


Figure 6. Measured NMSE as a function of processing speed T^{-1} for conventional (black) and proposed (red) RCs.

4.2. Handwritten Digit Recognition

To further verify the advantage of the proposed RC, the handwritten digit recognition task is adopted to test the word error rate performance [38]. The 28×28 images to be recognized show handwritten integers from 0 to 9. The images are taken from the MNIST data base, where 900 images are for training and 100 images are for testing. The desired training outputs are classifiers that have ten dimensional vector of ten digits. The classifier related to digit contains one value of 1 in the corresponding position, and the remaining nine values are all -1 . The mask consists of 0.51, 0.49, and 0 where the first two have equal probability of 0.01. In this task, the virtual node number is 400. Then, the image 28×28 is masked by 400×28 dimensional matrix mask in the input layer. The three-fold crossfold-validation is adopted to decrease the impact of division of image data in which the procedure of training and testing is repeated three times using different subsets. The evaluation index is word error rate (WER) which is defined using $WER = im_{wrong} / im_{total}$ [6,35].

Figure 7 compares the performance of proposed RC to the conventional one using the same configuration as in Figure 3 excepting for $\theta = 4$ ps and $k_i = 10$ ns⁻¹. The recognition results of 0–9 are displayed in color of white and black. The white square in corresponding position depicts right recognition. Obviously, it is easier to recognize the digits using the proposed RC than the conventional one. Comparing Figure 7a,b, the WER is reduced from 0.32 to 0.16 by using proposed RC with a relative high processing speed of about $T^{-1} = 625$ MSample/s. However, better performance can be achieved in conventional RC is much slower processing speed is adopted.

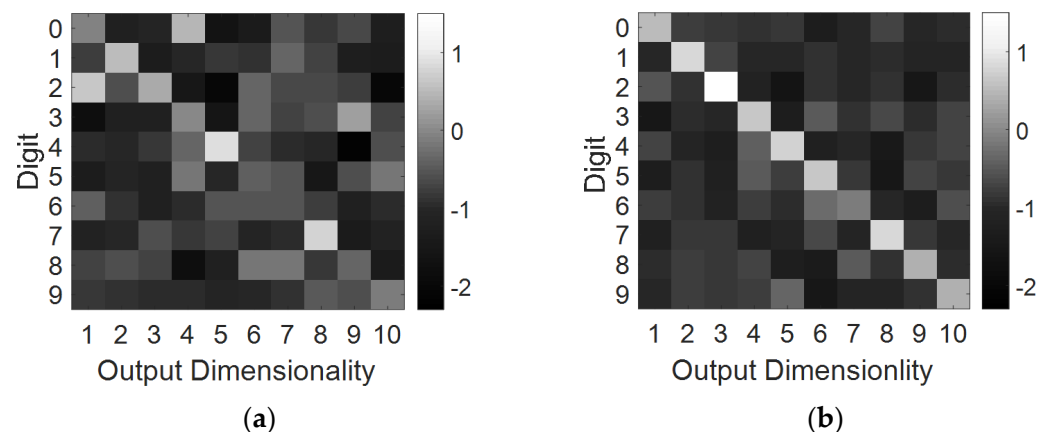


Figure 7. Handwritten digit recognition of 0–9 using (a) conventional RC and (b) proposed RC. The interval of $\theta = 4$ ps corresponds to a processing speed of about $T^{-1} = 625$ MSample/s.

5. Discussion

It is worth mentioning that some reported works have improved the processing speed up to 10 GSample/s in time-series prediction by taking advantage of short photon lifetime using particular lasers [15,23]. In addition, the NMSE from those works are usually in the order of 0.01. Practically, using optical injection is an universal approach to manipulate the carrier-photon resonance. Hence, our proposed method could be compatible to those particular lasers for achieving further improvement on both processing speed and NMSE.

6. Conclusions

In summary, a delay-laser-based RC under optical injection is proposed and numerically investigated. The optical injection is introduced to the response laser in the reservoir layer. Study of the response laser dynamics reveals an acceleration of the transient response. The chaotic time-series prediction task and handwritten digit recognition are adopted to test the improvement. The results show that the prediction error is significantly reduced and stabilized in high processing speed range by using proper injection parameters. Comparing

to the conventional RC, the proposed RC enhances the processing speed by an order of magnitude of about 5 GSample/s for NMSE below 0.006. The advantage of using proposed RC is also verified by using another task of handwritten digit recognition, where better WER is achieved.

Author Contributions: Z.L. and S.-S.L. contributed to the idea and the writing of the manuscript. X.Z., W.P. and L.Y. contributed to the reviewing and editing of the manuscript. All authors have read and agreed to the published version of the manuscript.

Funding: This research is funded by National Key Research and Development Program of China (2019YFB1803500), and National Natural Science Foundation of China (NSFC) (61905204).

Institutional Review Board Statement: Not applicable.

Informed Consent Statement: Not applicable.

Data Availability Statement: Not applicable.

Conflicts of Interest: The authors declare no conflict of interest.

References

1. Scardapane, S.; Gallicchio, C.; Micheli, A. Guest Editorial: Trends in Reservoir Computing. *Cogn. Comput.* **2021**, 1–2. [[CrossRef](#)]
2. Van der Sande, G.; Brunner, D.; Soriano, M.C. Advances in photonic reservoir computing. *Nanophotonics* **2017**, *6*, 561–576. [[CrossRef](#)]
3. Woods, D.; Naughton, T. Photonic neural networks. *Nat. Phys.* **2012**, *8*, 257–259. [[CrossRef](#)]
4. Lukoševičius, M.; Jaeger, S.; Schrauwen, H.B. Reservoir Computing Trends. *Künstl. Intell.* **2012**, *26*, 365–371. [[CrossRef](#)]
5. Sunada, S.; Uchida, A. Photonic reservoir computing based on nonlinear wave dynamics at microscale. *Sci. Rep.* **2019**, *9*, 19078. [[CrossRef](#)]
6. Appeltant, L.; Soriano, M.C.; Van der Sande, G.; Danckaert, J.; Massar, S.; Dambre, J.; Schrauwen, B.; Mirasso, C.R.; Fischer, I. Information processing using a single dynamical node as complex system. *Nat. Commun.* **2011**, *2*, 468. [[CrossRef](#)] [[PubMed](#)]
7. Brunner, D.; Soriano, M.C.; Mirasso, C.R.; Fischer, I. Parallel photonic information processing at gigabyte per second data rates using transient states. *Nat. Commun.* **2013**, *4*, 1364. [[CrossRef](#)] [[PubMed](#)]
8. Jaeger, H.; Haas, H. Harnessing nonlinearity: Predicting chaotic systems and saving energy in wireless communication. *Science* **2004**, *304*, 78–80. [[CrossRef](#)] [[PubMed](#)]
9. Hou, Y.S.; Xia, G.Q.; Jayaprasath, E. Parallel information processing using a reservoir computing system based on mutually coupled semiconductor lasers. *Appl. Phys.* **2020**, *40*, 126. [[CrossRef](#)]
10. Nguimdo, R.M.; Verschaffelt, G.; Danckaert, J.; Van der Sande, G. Simultaneous Computation of Two Independent Tasks Using Reservoir Computing Based on a Single Photonic Nonlinear Node with Optical Feedback. *IEEE Trans. Neural Netw. Learn. Syst.* **2015**, *26*, 3301–3307. [[CrossRef](#)] [[PubMed](#)]
11. Guo, X.X.; Xiang, S.Y.; Zhang, Y.H. Enhanced memory capacity of a neuromorphic reservoir computing system based on a VCSEL with double optical feedbacks. *Sci. China Inf. Sci.* **2020**, *63*, 160407. [[CrossRef](#)]
12. Harkhoe1, K.; Van der Sande, G. Delay-Based Reservoir Computing Using Multimode Semiconductor Lasers: Exploiting the Rich Carrier Dynamics. *IEEE J. Sel. Top. Quantum Electron.* **2019**, *25*, 1502909. [[CrossRef](#)]
13. Guo, X.X.; Xiang, S.Y.; Zhang, Y.H.; Lin, L.; Wen, A.J.; Hao, Y. Polarization Multiplexing Reservoir Computing Based on a VCSEL with Polarized Optical Feedback. *IEEE J. Sel. Top. Quantum Electron.* **2020**, *26*, 1700109. [[CrossRef](#)]
14. Bueno, J.; Brunner, D.; Soriano, M.C.; Fischer, I. Conditions for reservoir computing performance using semiconductor lasers with delayed optical feedback. *Opt. Express* **2017**, *25*, 2401–2412. [[CrossRef](#)] [[PubMed](#)]
15. Guo, X.X.; Xiang, S.Y.; Zhang, Y.H.; Lin, L.; Wen, A.J.; Hao, Y. High-Speed Neuromorphic Reservoir Computing Based on a Semiconductor Nanolaser with Optical Feedback Under Electrical Modulation. *IEEE J. Sel. Top. Quantum Electron.* **2020**, *26*, 1500707. [[CrossRef](#)]
16. Larger, L.; Baylón-Fuentes, A.; Martinenghi, R.; Udaltsov, V.S.; Chembo, Y.K.; Jacquot, M. High-speed photonic reservoir computing using a time-delay-based architecture: Million words per second classification. *Phys. Rev. X* **2017**, *7*, 011015. [[CrossRef](#)]
17. Yue, D.Z.; Wu, Z.M.; Hou, Y.S.; Hu, C.X.; Jiang, Z.F.; Xia, G.Q. Reservoir Computing Based on Two Parallel Reservoirs under Identical Electrical Message Injection. *IEEE Photon. J.* **2021**, *13*, 7800311. [[CrossRef](#)]
18. Martinenghi, R.; Rybalko, S.; Jacquot, M.; Chembo, Y.; Larger, L. Photonic nonlinear transient computing with multiple-delay wavelength dynamics. *Phys. Rev. Lett.* **2012**, *108*, 244101. [[CrossRef](#)]
19. Nguimdo, R.; Verschaffelt, G.; Danckaert, J.; Van der Sande, G. Fast photonic information processing using semiconductor lasers with delayed optical feedback: Role of phase dynamics. *Opt. Express* **2014**, *7*, 72–86. [[CrossRef](#)]
20. Nakayama, J.; Kanno, K.; Uchida, A. Laser dynamical reservoir computing with consistency: An approach of a chaos mask signal. *Opt. Express* **2016**, *24*, 79–92. [[CrossRef](#)]

21. Kuriki, Y.; Nakayama, J.; Takano, K.; Uchida, A. Impact of input mask signals on delay-based photonic reservoir computing with semiconductor lasers. *Opt. Express* **2018**, *26*, 77–88. [[CrossRef](#)] [[PubMed](#)]
22. Duport, F.; Schneider, B.; Smerieri, A.; Haelterman, M.; Massar, S. All-optical reservoir computing. *Opt. Express* **2012**, *20*, 783–795. [[CrossRef](#)] [[PubMed](#)]
23. Huang, Y.; Zhou, P.; Yang, Y.; Li, N.Q. High-speed photonic reservoir computer based on a delayed Fano laser under electrical modulation. *Opt. Lett.* **2021**, *46*, 35–38. [[CrossRef](#)] [[PubMed](#)]
24. Guo, X.X.; Xiang, S.Y.; Zhang, Y.H.; Lin, L.; Wen, A.J.; Hao, Y. Four-channels reservoir computing based on polarization dynamics in mutually coupled VCSELs system. *Opt. Express* **2019**, *27*, 23293–23306. [[CrossRef](#)] [[PubMed](#)]
25. Vatin, J.; Rontani, D.; Sciamanna, M. Enhanced performance of a reservoir computer using polarization dynamics in VCSELs. *Opt. Lett.* **2018**, *43*, 4497–4500. [[CrossRef](#)] [[PubMed](#)]
26. Lang, R.; Kobayashi, K. External optical feedback effects on semiconductor injection laser properties. *IEEE J. Quantum Electron.* **1980**, *16*, 347–355. [[CrossRef](#)]
27. Uchida, A. *Optical Communication with Chaotic Lasers, Applications of Nonlinear Dynamics and Synchronization*; Wiley-VCH: Hoboken, NJ, USA, 2012; pp. 156–192.
28. Chan, S.C.; Hwang, S.K.; Liu, J.M. Period-one oscillation for photonic microwave transmission using an optically injected semiconductor laser. *Opt. Express* **2007**, *15*, 14921–14935. [[CrossRef](#)]
29. Li, S.; Chan, S. Chaotic Time-Delay Signature Suppression in a Semiconductor Laser with Frequency-Detuned Grating Feedback. *IEEE J. Sel. Top. Quantum Electron.* **2015**, *21*, 541–552.
30. Simpson, T.B.; Liu, J.M.; Gavrielides, A. Bandwidth enhancement and broadband noise reduction in injection-locked semiconductor laser. *IEEE Photon. Technol. Lett.* **1995**, *7*, 709–711. [[CrossRef](#)]
31. Wang, J.; Haldar, M.K.; Li, L.; Mendis, F.V.C. Enhancement of modulation bandwidth of laser diodes by injection locking. *IEEE Photon. Technol. Lett.* **1996**, *8*, 34–36. [[CrossRef](#)]
32. Harkhoe, K.; Van der Sande, G. Task-Independent Computational Abilities of Semiconductor Lasers with Delayed Optical Feedback for Reservoir Computing. *Photonics* **2019**, *6*, 124. [[CrossRef](#)]
33. Hübner, U.; Abraham, N.; Weiss, C. Dimensions and entropies of chaotic intensity pulsations in a single-mode far-infrared NH₃ laser. *Phys. Rev. A* **1989**, *11*, 54–65.
34. Weigend, A.S.; Gershenfeld, N.A. *Time Series Prediction: Forecasting the Future and Understanding the Past*; 1993. Available online: <http://wwwpsych.stanford.edu/~jandreas/Time-Series/SantaFe.html> (accessed on 31 March 2022).
35. Paquot, Y.; Duport, F.; Smerieri, A. Optoelectronic Reservoir Computing. *Sci. Rep.* **2012**, *2*, 87–92. [[CrossRef](#)] [[PubMed](#)]
36. Ortín, S.; Pesquera, L. Delay-based reservoir computing: Tackling performance degradation due to system response time. *Opt. Lett.* **2020**, *45*, 905–908. [[CrossRef](#)] [[PubMed](#)]
37. Yue, D.Z.; Xia, G.Q.; Iayaprasath, E.; Yue, D.Z.; Yang, W.Y.; Wu, Z.M. Prediction and classification performance of reservoir computing system using mutually delay-coupled semiconductor lasers. *Opt. Commun.* **2019**, *433*, 215–220.
38. Nguimdo, R.M.; Antonik, P.; Marsal, N.; Rontani, D. Impact of optical coherence on the performance of large-scale spatiotemporal photonic reservoir computing systems. *Opt. Express* **2020**, *28*, 27989–28005. [[CrossRef](#)]